Christian Marinus Huber*, Sarah Therre-Mohr, Lars Hageroth, Christian Heim, Helmut Ermert, Stefan J. Rupitsch, Ingrid Ullmann, Marc Fournelle, Steffen Tretbar, and Stefan Lyer

3D Magnetomotive Displacement Estimation of Magnetic Nanoparticles using a Matrix Transducer

https://doi.org/10.1515/cdbme-2025-0138

Abstract: Magnetic Drug Targeting (MDT) is a promising technique for local chemotherapy, employing magnetic nanoparticles (MNPs) and an external electromagnet to concentrate chemotherapeutic agents at tumor sites. Achieving complete tumor perfusion with the drug requires precise control over MNP distribution, which can be optimized by repositioning the electromagnet. However, this process needs a therapy monitoring system capable of 3D mapping of MNP distribution within the tumor. While ultrasound-based imaging techniques, particularly magnetomotive ultrasound (MMUS), have been shown to effectively track MNP accumulation in 2D, a full 3D characterization remains challenging. In this study, we employ a matrix transducer combined with a slice-by-slice 2D global ultrasound elastography (GLUE) approach to reconstruct a 3D magnetomotive displacement map, enabling improved visualization of the MNP distribution.

Keywords: Ultrasound, Cancer Therapy, Magnetic Nanoparticles, Elastography, Motion Estimation

***Corresponding author: Christian Marinus Huber,** Department of Otorhinolaryngology, Head and Neck Surgery, Section of Experimental Oncology and Nanomedicine, Professorship for AI-Controlled Nanomaterials, Universitätsklinikum Erlangen, Erlangen, Germany; Institute of Microwaves and Photonics (LHFT), Friedrich-Alexander-Universität Erlangen-Nürnberg, Erlangen, Germany e-mail: Christian.ch.huber@fau.de
Helmut Ermert, Stefan Lyer, Department of Otorhinolaryngology, Head and Neck Surgery, Section of Experimental Oncology and Nanomedicine, Professorship for AI-Controlled Nanomaterials, Universitätsklinikum Erlangen, Erlangen, Germany
Lars Hageroth, Ingrid Ullmann, Institute of Microwaves and Photonics (LHFT), Friedrich-Alexander-Universität Erlangen-Nürnberg, Erlangen, Germany
Sarah Therre-Mohr, Marc Fournelle, Steffen Tretbar, Department Ultrasound, Fraunhofer Institute for Biomedical Engineering (IBMT), Sulzbach/Saar, Germany
Sarah Therre-Mohr, Department of Molecular and Cellular Biotechnology, Saarland University, Saarbrücken, Germany
Christian Heim, Stefan J. Rupitsch, Department of Microsystems Engineering (IMTEK), Laboratory for Electrical Instrumentation and Embedded Systems (EMES), University of Freiburg, Freiburg, Germany

1 Introduction

Cancer remains the second leading cause of mortality worldwide, surpassed only by cardiovascular diseases, claiming approximately 20 million lives annually [1]. Despite being a standard treatment, chemotherapy is associated with significant systemic side effects due to its non-specific distribution. Chemotherapeutic agents are typically administered intravenously, affecting not only malignant tissues but also healthy cells, leading to adverse effects such as nausea, hair loss, and immunosuppression.

A promising advancement in targeted drug delivery involves the use of nanoscale drug carriers [2]. In the case of Magnetic Drug Targeting (MDT) [3], magnetic nanoparticles (MNPs) serve as drug carriers that can be accumulated at the tumor site using an external electromagnet. Compared to non-magnetic nanoparticles, MNPs offer the advantage of controlled accumulation at the target location [4]. The animal study demonstrated that MDT results in higher intratumoral concentrations of chemotherapeutic agents while reducing off-target toxicity. Additionally, the study reported complete tumor recession after a single MDT application for half of the animals.

For effective tumor treatment, complete perfusion of the tumor with the drug is required. To achieve this during MDT treatment, it is essential to be able to record the 3-dimensional (3D) distribution of the particles in real time in order to be able to dynamically reposition the external electromagnet. Magnetic resonance imaging (MRI) is not compatible with the strong magnetic fields used for MNP accumulation, and while Magnetic Particle Imaging (MPI) holds potential for this application, it remains in an early research phase [5]. Ultrasound-based imaging techniques [6], particularly magnetomotive ultrasound (MMUS) [7], have been shown to successfully visualize MNP distribution during MDT in two dimensions (2D) using a linear ultrasound array [8].

In this study, we employed a matrix transducer to extend MMUS imaging to three dimensions, enabling 3D magnetomotive displacement estimation for improved therapy monitoring and optimized MDT treatment strategies.

2 Methods and Materials

MMUS is an ultrasound-based imaging technique for visualizing the distribution of MNPs within tissue. This is achieved by applying a time-varying magnetic field using the accumulation electromagnet, which induces motion in MNP-perfused tissue. An ultrasound probe captures beamformed radio-frequency (RF) data to track this tissue displacement. Since the MNP-induced motion follows the pattern of the applied magnetic field, tissue movement serves as a proxy for estimating MNP distribution.

2.1 Displacement Estimation

To estimate displacement in 3D, we employ an ultrasound matrix probe combined with a slice-by-slice approach. For each slice of the beamformed RF-data, 2D global ultrasound elastography (2D-GLUE) [9, 10] was utilized to compute the axial displacement. A detailed description of 2D-GLUE can be found in [9], while a brief overview is provided here.

Conventional displacement estimation in ultrasound elastography typically relies on one-dimensional or window-based correlation methods. In contrast, 2D-GLUE estimates the two-dimensional displacement globally by considering all samples within two RF-data slices (I_1, I_2) across axial (a_i) and lateral (l_i) directions for all $i = 1, \ldots, m$ samples of all $j = 1, \ldots, n$ RF-lines. This is by using an initial displacement map and by minimizing the cost function

$$
\begin{aligned}
&C_S(\Delta a_{1,1}, \ldots, \Delta a_{m,n}, \Delta l_{1,1}, \ldots, \Delta l_{m,n}) \\
&= \sum_{j=1}^{n} \sum_{i=1}^{m} \Big\{ [I_1(i,j) - I_2(i + a_{i,j} + \Delta a_{i,j}, j + l_{i,j} + \Delta l_{i,j})]^2 \\
&\qquad + \alpha_1 (a_{i,j} + \Delta a_{i,j} - a_{i-1,j} - \Delta a_{i-1,j})^2 \\
&\qquad + \beta_1 (l_{i,j} + \Delta l_{i,j} - l_{i-1,j} - \Delta l_{i-1,j})^2 \\
&\qquad + \alpha_2 (a_{i,j} + \Delta a_{i,j} - a_{i,j-1} - \Delta a_{i,j-1})^2 \\
&\qquad + \beta_2 (a_{i,j} + \Delta a_{i,j} - a_{i,j-1} - \Delta a_{i,j-1})^2, \qquad (1)
\end{aligned}
$$

where $\Delta a_{i,j}$ and $\Delta l_{i,j}$ represent sub-sample displacement corrections. The regularization parameters α_1 and β_1 enforce smoothness constraints on axial displacement along the axial and lateral directions, while α_2 and β_2 do so for lateral displacement. In this study, only the axial displacement was utilized.

A Taylor series expansion of the cost function was employed to construct a linear system of equations, which was then solved using numerical optimization techniques. An openly available implementation (https://users.encs.concordia.ca/ hrivaz/Ultrasound_Elastography/) was used for this purpose.

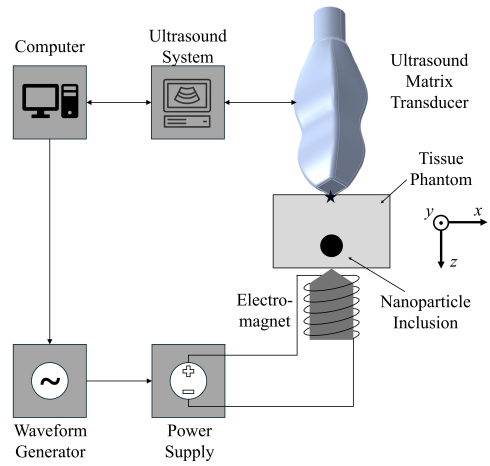

Fig. 1: Illustration of the experimental setup. The origin of the used coordinate system is marked with a star symbol below the transducer.

This approach enables accurate axial displacement estimation using only two frames.

2.2 Experimental Setup

The experimental setup (see Fig. 1) consisted of an electromagnet powered by a dedicated power supply (Sorensen DLM 40-75E), which is controlled by a signal generator (Agilent 33220A). This configuration generates a sinusoidal time-varying magnetic field at 0.5 Hz, with a magnetic flux density of 1 T at the pole tip and a field gradient of 72 T/m [11].

Positioned above the electromagnet was an ultrasound phantom, fabricated following protocols from [12, 13]. The phantom's outer part consisted of 10 weight percent (wt%) polyvinyl alcohol (PVA, Kuraray, Elvanol 71-30) powder, 1 wt% silica gel, and 89 wt% deionized water. The MNP-infused region was created by replacing water with a dextran-coated magnetic nanoparticle (MNP) suspension at an iron content of 5 mg Fe/mL, followed by two freeze-thaw cycles to enhance structural stability. The outer phantom dimensions were $(x, y, z) = (45, 25, 45)$ mm, with an embedded cylindrical inclusion. The inclusion's circular base was placed in the xz-plane with $(x, z) = (-1, 34)$ mm and a 10 mm diameter, and extended 25 mm along the y-axis.

A matrix ultrasound transducer (Vermon, 3 MHz, 32 × 32 elements, 0.3 × 0.3 mm pitch) was positioned above the phantom and connected to a 1024-channel Digital Phased Array System (DiPhAS, Fraunhofer IBMT) [14]. The transducer operated in plane wave compounding mode using nine angled plane waves, achieving a data acquisition rate of 7 Hz. For displacement estimation, two beamformed datasets were ac-

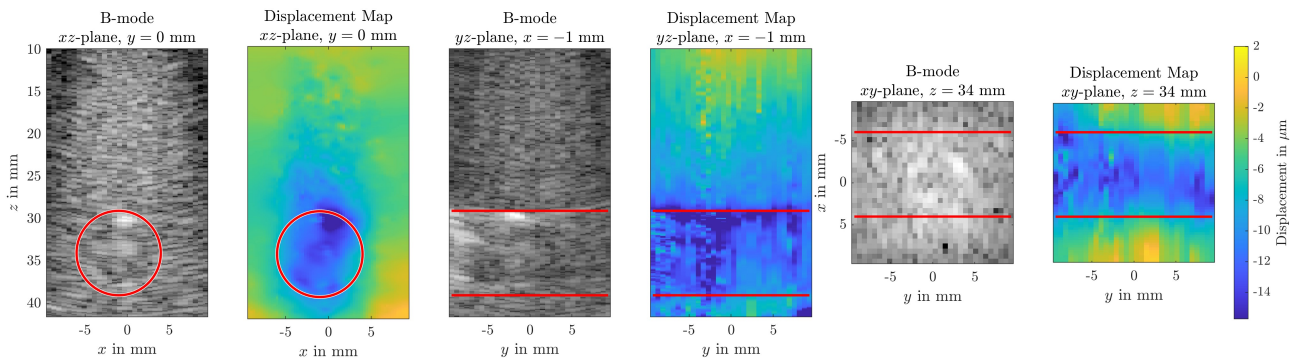

Fig. 2: Results of the magnetomotive displacement estimation for planes xy at $z = 34$ mm, xz at $y = 0$ mm and yz at $x = 0$ mm. The red lines indicate the position of the nanoparticle inclusion.

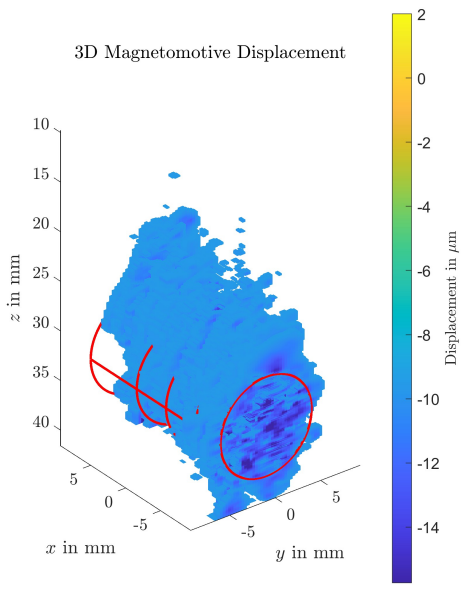

Fig. 3: Results of the magnetomotive displacement estimation in 3D (values above -10 μm are transparent). Red lines and circles indicate the nanoparticle inclusion.

quired, corresponding to the time points when the magnetic field reached its minimum and maximum, allowing for maximal magnetomotive displacement.

3 Results and Discussions

The results of the magnetomotive displacement estimation using a matrix transducer and the 2D-GLUE algorithm are presented in Fig. 2 and Fig. 3. Fig. 2 illustrates the estimated displacement in three orthogonal 2D planes: the xy-plane at $z = 34$ mm, the xz-plane at $y = 0$ mm and the yz-plane at $x = -1$ mm. The nanoparticle inclusion was positioned slightly off-center at $(x, z) = (-1, 34)$ mm and extends along the y-direction.

In the xz-plane, the inclusion exhibited a circular shape, which was faintly visible in both the B-mode image and the displacement map. Due to the applied magnetic force, the inclusion underwent displacement, which in turn induced motion in the surrounding mechanically coupled non-nanoparticle-perfused tissue. Additionally, a counteracting displacement is observed beneath the inclusion.

In the yz- and xy-planes, the nanoparticle inclusion appeared as a rectangular shape, which was similarly distinguishable in both the B-mode and displacement maps. Fig. 3 provides a 3D visualization of the axial displacement map, displaying only displacements smaller than -10 μm to enhance the visibility of the nanoparticle-laden region. The cylindrical inclusion was discernible, though, as previously mentioned, the induced displacement extends beyond the nanoparticle-infused region due to mechanical coupling with the surrounding phantom material. The estimated displacement within the nanoparticle-laden tissue fell within the range of -10 to -15 μm, consistent with previous studies employing standard linear array transducers [12, 15].

Both figures demonstrate reliable displacement estimation in each xz-slice. However, discontinuities were observed along the y-direction. This can be attributed to the limitations of the 2D-GLUE algorithm, which exclusively processes 2D datasets without accounting for inter-slice continuity in the y-axis.

4 Conclusion

In this study, three-dimensional magnetomotive displacement maps were generated using a matrix transducer in combination with a slice-by-slice 2D-GLUE algorithm. The estimated displacements were consistent with values reported in previous studies, demonstrating the potential of matrix transducers for magnetomotive ultrasound imaging. The applied slice-by-slice

2D-GLUE approach produced smooth displacement maps in each xz-slice. However, discontinuities were observed in the orthogonal planes due to the inherent limitations of independent processing of 2D datasets.

Despite these limitations, we successfully demonstrated the feasibility of mapping axial magnetomotive displacements in 3D using a matrix transducer. This imaging approach has the potential to enhance tumor perfusion monitoring during Magnetic Drug Targeting (MDT) and could further improve the quantification of nanoparticle distribution via inverse MMUS, which will be investigated in future studies. Additionally, the implementation and evaluation of the 3D-GLUE algorithm [16, 17] for fully volumetric MMUS imaging will be explored as part of ongoing research.

Author Statement

Research funding: The authors gratefully acknowledge the financial support of the Deutsche Forschungsgemeinschaft (DFG) - project number 452821018 and the Julitta und Richard Müller Stiftung. Conflict of interest: Authors state no conflict of interest.

References

[1] Jacques Ferlay, Murielle Colombet, Isabelle Soerjomataram, Donald M. Parkin, Marion Piñeros, Ariana Znaor, and Freddie Bray. Cancer statistics for the year 2020: An overview. *International journal of cancer*, 2021.

[2] Agnieszka Z. Wilczewska, Katarzyna Niemirowicz, Karolina H. Markiewicz, and Halina Car. Nanoparticles as drug delivery systems. *Pharmacological reports : PR*, 64(5):1020–1037, 2012.

[3] Rainer Tietze, Stefan Lyer, Stephan Dürr, Tobias Struffert, Tobias Engelhorn, Marc Schwarz, Elisabeth Eckert, Thomas Göen, Serhiy Vasylyev, Wolfgang Peukert, Frank Wiekhorst, Lutz Trahms, Arnd Dörfler, and Christoph Alexiou. Efficient drug-delivery using magnetic nanoparticles–biodistribution and therapeutic effects in tumour bearing rabbits. *Nanomedicine : nanotechnology, biology, and medicine*, 9(7):961–971, 2013.

[4] Angelika S. Thalmayer, Lucas Fink, and Georg Fischer. Experimental and simulative characterization of a hybrid magnetic array for steering superparamagnetic nanoparticles in drug targeting. *IEEE transactions on bio-medical engineering*, 72(3):940–952, 2025.

[5] Tae-Hyun Shin, Youngseon Choi, Soojin Kim, and Jinwoo Cheon. Recent advances in magnetic nanoparticle-based multi-modal imaging. *Chemical Society reviews*, 44(14):4501–4516, 2015.

[6] Christian Marinus Huber, Theo Z. Pavan, Ingrid Ullmann, Christian Heim, Stefan J. Rupitsch, Martin Vossiek, Christoph Alexiou, Helmut Ermert, and Stefan Lyer. A review on ultrasound-based methods to image the distribution of magnetic nanoparticles in biomedical applications. *Ultrasound in medicine & biology*, 51(2):210–234, 2025.

[7] Junghwan Oh, Marc D. Feldman, Jeehyun Kim, Chris Condit, Stanislav Emelianov, and Thomas E. Milner. Detection of magnetic nanoparticles in tissue using magneto-motive ultrasound. *Nanotechnology*, 17(16):4183–4190, 2006.

[8] Michael Fink, Stefan J. Rupitsch, Helmut Ermert, and Stefan Lyer. In vivo study on magnetomotive ultrasound imaging in the framework of nanoparticle based magnetic drug targeting. *Current Directions in Biomedical Engineering*, 6(3):543–546, 2020.

[9] Hoda Sadat Hashemi and Hassan Rivaz. Global time-delay estimation in ultrasound elastography. *IEEE transactions on ultrasonics, ferroelectrics, and frequency control*, 64(10):1625–1636, 2017.

[10] Hassan Rivaz, Emad M. Boctor, Michael A. Choti, and Gregory D. Hager. Real-time regularized ultrasound elastography. *IEEE transactions on medical imaging*, 30(4):928–945, 2011.

[11] Christoph Alexiou, Rainer Tietze, Eveline Schreiber, Roland Jurgons, Heike Richter, Lutz Trahms, Helene Rahn, Stefan Odenbach, and Stefan Lyer. Cancer therapy with drug loaded magnetic nanoparticles—magnetic drug targeting. *Journal of Magnetism and Magnetic Materials*, 323(10):1404–1407, 2011.

[12] Christian Marinus Huber, Christian Heim, Jiaqi Li, Helmut Ermert, Stefan J. Rupitsch, Ingrid Ullmann, and Stefan Lyer. Magnetomotive displacement of magnetic nanoparticles in different tissue phantoms. *Current Directions in Biomedical Engineering*, 10(4):324–327, 2024.

[13] C. Heim, T. Saleem, S. J. Rupitsch, C. M. Huber, S. Lyer, H. Ermert, and I. Ullmann. D1.4 - modelling and construction of complex shaped polyvinyl alcohol based ultrasound phantoms for inverse magnetomotive ultrasound imaging. In *Vorträge*, pages 313–318. AMA Service GmbH, Von-Münchhausen-Str. 49, 31515 Wunstorf, 2024.

[14] Christoph Risser, Holger Hewener, Marc Fournelle, Heinrich Fonfara, Selina Barry-Hummel, Steffen Weber, Daniel Speicher, and Steffen Tretbar. Real-time volumetric ultrasound research platform with 1024 parallel transmit and receive channels. *Applied Sciences*, 11(13):5795, 2021.

[15] Ernesto Edgar Mazon Valadez, João Henrique Uliana, Thiago Tiburcio Vicente, Antonio Adilton Oliveira Carneiro, and Theo Zeferino Pavan. Fully-automated theranostic system integrating magnetomotive ultrasound and magnetic hyperthermia. *IEEE Transactions on Instrumentation and Measurement*, 74:1–11, 2025.

[16] Hoda S. Hashemi, Mohammad Honarvar, Tim Salcudean, and Robert Rohling. 3d global time-delay estimation for shear-wave absolute vibro-elastography of the placenta. *Annual International Conference of the IEEE Engineering in Medicine and Biology Society. IEEE Engineering in Medicine and Biology Society. Annual International Conference*, 2020:2079–2083, 2020.

[17] Hoda S. Hashemi, Shahed K. Mohammed, Qi Zeng, Reza Zahiri Azar, Robert N. Rohling, and Septimiu E. Salcudean. 3-d ultrafast shear wave absolute vibro-elastography using a matrix array transducer. *IEEE transactions on ultrasonics, ferroelectrics, and frequency control*, 70(9):1039–1053, 2023.